Research on Industrial Production Defect Detection Method Based on Machine Vision Technology in Industrial Internet of Things

Limin Jia[1], Yang Wang[2*]

[1] Shenzhen Decard Smartcard Tech Co., Ltd., Shenzhen 518055, China
[2] School of Electronic and Communication Engineering, Shenzhen Polytechnic, Shenzhen 518055, China

Corresponding Author Email: wyang@szpt.edu.cn

ABSTRACT

The realization of automatic operation of production by the industrial Internet of Things needs the functional assistance of machine vision technology. Different from the recognition and detection of some known features, it is difficult to realize defect detection in machine vision applications. Therefore, this article studies the industrial production defect detection method based on machine vision technology in industrial Internet of Things. Firstly, in the second chapter, the images of industrial products collected by machine vision system are preprocessed and thinned to obtain more ideal detection accuracy and measurement accuracy. The methods of image binarization, morphological processing, thinning and burr elimination are given in detail. In the third chapter, product defect detection model is constructed based on U-Net network, and residual structure, hole convolution module, strip pooling module and attention mechanism module are introduced to optimize the network model. Experimental results verify the effectiveness of the model for product defect detection.

1. INTRODUCTION

In recent years, China's advanced manufacturing industry has developed rapidly, and advanced concepts and technologies such as Intelligent Manufacturing in 2025 and Industrial Internet of Things are gradually merging into the manufacturing industry. Equipment in the production environment of industrial Internet of Things undertakes a large number of production tasks every day [1-8]. If all links of incoming materials, processing, assembly, packaging and logistics are highly automated, the equipment on the production line needs accurate operation, quick response and close networking cooperation, where the functional assistance of machine vision technology plays a key role [9-13]. Machine vision can reliably identify various targets in the production process, and is helpful for the control system to make accurate and rapid production decisions [14-21]. Different from the recognition and detection of some known features, it is difficult to realize defect detection in machine vision applications. Because there are many kinds of defects in products and their characteristics are unpredictable. It is of great research value to study the industrial production defect detection method based on machine vision technology in industrial Internet of Things.

In order to meet the increasing demand for high-quality products and solve the shortcomings of manual quality control procedures, the use of intelligent visual inspection system is becoming more and more important for the deployment of production lines. Reference [22] proposes a framework composed of three mind maps to capture the essence of defect detection, and proposes manufacturing defect classification based on visual attributes. An empirical recommendation formula based on three image metrics such as entropy, universal quality index (UQI) and Rosenberger is proposed to judge the performance of the method in a given image category. Reference [23] discusses the effectiveness of data enhancement methods deployed in many convolution neural network algorithms in determining wood defects of four kinds of wood in Malaysia. A series of morphological transformations, including x-reflection and rotation, are performed in the wood defect enhancement data set to help CNN model training and generate the best CNN model that provides the best classification performance when determining wood defects. Experimental results show that the proposed method improves the classification performance of CNN algorithm in wood defect recognition, and solves the challenges of unbalanced and limited datasets. Reference [24] introduces Hough Transform, which is robust to point noise, to automatically identify the linear features of magnetic particle testing (MPI) caused by defects. However, the algorithm can not distinguish FMPI and MPI with similar shapes. The density of the normal component of magnetic flux on the sample surface is calculated by finite element analysis to evaluate the possibility of FMPI.

This article studies the industrial production defect detection method based on machine vision technology in industrial Internet of Things. Firstly, in the second chapter, the images of industrial products collected by machine vision system are preprocessed and thinned to obtain more ideal detection accuracy and measurement accuracy. The methods of image binarization, morphological processing, thinning and burr elimination are given in detail. In the third chapter, product defect detection model is constructed based on U-Net network, and residual structure, hole convolution module, strip pooling module and attention mechanism module are introduced to optimize the network model. Experimental

results verify the effectiveness of the model for product defect detection.

2. THINNING OF INDUSTRIAL PRODUCTION IMAGES

In the process of collecting image data of industrial products by machine vision system, if the production environment changes, such as the deviation of optics, lighting or product specifications, or the product is quite different from the background color, the image data distribution may change, that is, false defects such as water stains, illumination shadows and black spots, which are very similar to the actual defects, resulting in a large false detection rate. Therefore, this article aims to put forward a defect detection model of industrial products that can eliminate false defects, which is of great significance to the popularization and development of machine vision technology in industrial Internet of Things.

Before the defect recognition of industrial products, this article preprocesses and thins the images of industrial products collected by machine vision system to obtain more ideal detection accuracy and measurement accuracy. Firstly, this article distinguishes the defect characteristics of industrial products from other background impurities. The gray value of any point (a,b) in the defect image of industrial products is represented by $g(i,j)$, the gray value obtained after binarization is represented by $f(i,j)$, and the preset threshold value is represented by E. The following formula gives the image binarization formula:

$$f\left(i,j\right)=\begin{cases}0, g\left(i,j\right)<E\\255, g\left(i,j\right)\geq E\end{cases} \qquad (1)$$

For a product image with multiple defects, each defect must be marked to distinguish a single defect from the background area of the product image. In this article, defect marking is realized by filling small holes with the help of morphological theory. It is assumed that the boundary etching of target defects is expressed by ○ and the expansion is expressed by ⊕, the formula is as follows:

$$\left(\left(g\oplus\psi\right)\circ\psi\right) \qquad (2)$$

In order to eliminate the isolated noise pixels in the product image, this article introduces the opening operation, and the formula is as follows:

$$\left(\left(g\,!\,\psi\right)\oplus\psi\right) \qquad (3)$$

Further thin the product defects, with the thinning steps as follows:

STEP1: Count the number of pixels with a pixel value of 1 in 8 neighborhood. If the value is greater than 2 and less than 6, etch the pixels and convert them into background;

STEP2: Count the pixel value change of adjacent pixel points in 8 neighborhood. If only one pair of pixels change in 0-1 mode, etch the pixels and convert them into background;

STEP3: Count the pixel value of the adjacent pixel points in 8 neighborhood. If at least one pixel value is 0, etch the pixel point and convert it into background;

STEP4: Count the pixel values of the pixel points on the right and left and below the pixel point. If at least one pixel value is 0, etch the pixel point and convert it into background;

STEP5: Count the pixel values of the pixel points on the right and left and above the pixel point. If at least one pixel value is 0, etch the pixel point and convert it into background;

STEP6: Count the pixel values of the pixel points above and below the pixel points and on the left. If at least one pixel value is 0, etch the pixel point and convert it into background.

Repeat the above steps, and the 3×3 convolution kernel iterates continuously along the edge of the connected region to the center of the product defect image until no pixel points need to be etched, and then the image is the thinned product defect image.

The product defect image generated by the above steps not only ensures the connectivity of the thinned defects, but also retains abundant defect shape feature information. The burr at the end point of the defect can be eliminated by chain code tracking, and the specific implementation steps are described as follows:

STEP1: Traverse the thinned product defect image and search the position of defect node;

STEP2: Scan and chain code track the defective branch by taking the node position as the starting point until it reaches the other end node of the branch;

STEP3: Set the step threshold as X_0. If X_0 is larger than the scanning pixel step, the pixel point at the node is etched and converted into a background. If X_0 is smaller than the scanning pixel step, the next node and branch are scanned.

3. OPTIMIZATION OF DEFECT DETECTION MODEL IN INDUSTRIAL PRODUCTION

This article builds a product defect detection model based on U-Net network. The network has better segmentation effect, increases channel connection, and can connect the global information and local information of product images, which is suitable for extracting richer target product features. In particular, the optimization function of U-Net network is a random gradient descent function, which can effectively solve the problem that the traditional network model has poor effect on product boundary extraction. table 1 shows the U-Net network model architecture. Assuming that the value of position a in the l-th feature channel is represented by $\beta_l(a)$, the number of classes is represented by L, and the approximate maximum function is represented by $e_l(a)$, then the function definition formula is given by the following formula:

$$e_l\left(a\right)=\exp\left(\beta_l\left(a\right)\right)/\left(\sum_{l'=1}^{L}\exp\left(\beta_{l'}\left(a\right)\right)\right) \qquad (4)$$

Assuming that the true label of each pixel of the product defect image is represented by k and the weight of each pixel is represented by θ, the following formula gives the definition formula of the cross entropy penalty P for the deviation between each pixel $e_{k(a)}$ and 1 of the product defect image:

$$P=\sum_{a\in\Omega}\theta\left(a\right)\log\left(e_{k(a)}\left(a\right)\right) \qquad (5)$$

In the process of down-sampling, this article optimizes U-Net network based on residual structure, aiming at the problem

that the defect extraction features of traditional convolution neural network are not rich enough. Residual block is composed of two convolution layers, a batch normalization layer and commonly used activation functions. Assuming that the characteristics of the input of residual structure are represented by a, the learned residual is represented by $G(a)$, the expected output is represented by $F(a)$, the parameters are represented by Q, the input of k layer is represented by a_k, the output of $k+1$ layer is represented by a_{k+1}, and the nonlinear

activation function is represented by $E(a_k,Q_k)$, the following formula gives the residual structure expression based on the nonlinear mapping structure *Weight-layer*:

$$a_{k+1} = a_k + G(a_k, Q_k) \qquad (6)$$

When $G(a)=0$, $F(a)=a$, and the network can be regarded as an identity mapping, that is, a shortcut connection.
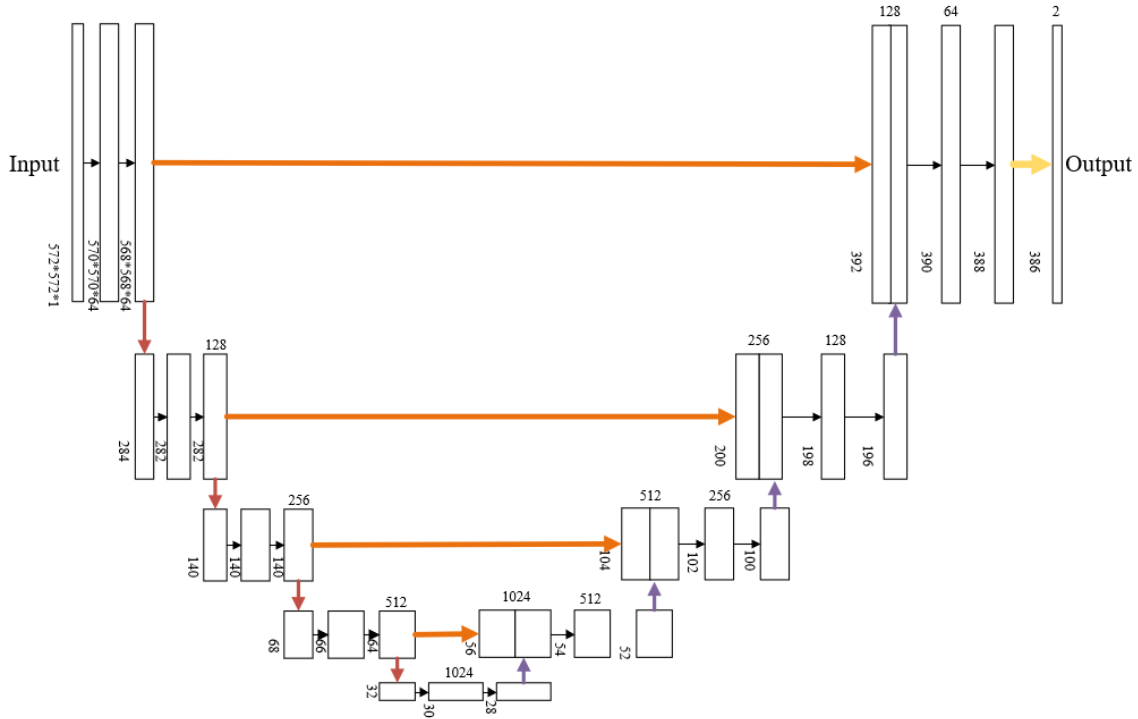

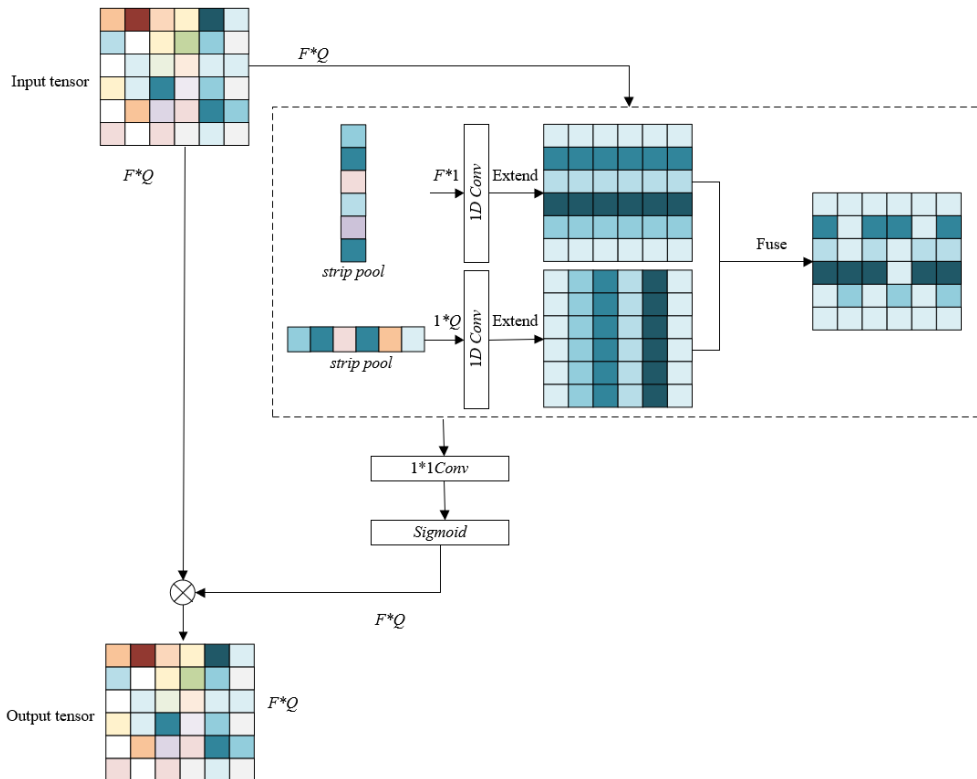**Figure 1.** U-Net network model architecture

Figure 2. Introducing stripe pooling module architecture

To solve the problem of large parameters of U-Net network, this article introduces a hole convolution module which can enlarge the receptive field to optimize it. The difference between hole convolution and normal convolution is that hole convolution can obtain a larger receptive field by increasing the number of holes in convolution layers with the same size of convolution kernel and step size, while keeping the size of feature map unchanged and the image resolution impaired, and it is effective in both one-dimensional space and two-dimensional space. Assuming that the size of convolution kernel is represented by l, the number of holes is represented by EN, and the size of receptive field is represented by G, the following formula gives the calculation formula of receptive field of hole convolution:

$$G = 2 \times (EN - 1) \times (l - 1) + l \tag{7}$$

This article studies the extraction of defects in industrial products. The shape of defects is uncertain, usually strip-shaped. Therefore, when extracting this kind of defect information, the traditional pooling method is not ideal for global and local information aggregation. This article thus introduces *Strip Pooling* to optimize U-Net network in order to obtain different-shaped defect features, especially strip-shaped defects, and reduce the amount of computation. Figure 2 shows the architecture of introducing stripe pooling module. Assuming that the two-dimensional tensor is represented by a and satisfies $a \in R^{F \times Q}$, the height and width of the space are represented by F and Q, respectively, and the output value of the horizontal strip is represented by $b^f \in R^F$, the following formula gives the horizontal stripe pooling formula for the Strip Pooling module:

$$b_i^f = \frac{1}{Q} \sum_{0 \leq j \leq q} a_{i,j} \tag{8}$$

Assuming that the output value of the vertical strips is expressed by $b^u \in R^Q$, the vertical strip pooling calculation formula is as follows:

$$b_i^u = \frac{1}{F} \sum_{0 \leq i \leq F} a_{i,j} \tag{9}$$

In order to accurately locate the specific location of defects in industrial products and improve the efficiency and accuracy of defect recognition, this article connects encoder and decoder based on attention mechanism module CA to complete the feature decoding of identified defects.

CA encodes the correlation between the channel information transmitted by network model and product defect characteristics through the location information of defects on industrial products. The process consists of two steps. The first step is information embedding. If the input feature a is given, each channel of the network model is encoded along the horizontal and vertical coordinates based on the merging kernel $(F,1)$ or $(1,Q)$. Assuming that the height and width of the input feature are represented by F and Q, respectively, the number of channels is represented by d, the output characteristics are represented by c_d, and the horizontal and vertical lengths are represented by i and j, then the following formula gives the output height of the d-th channel:

$$C_d^f (f) = \frac{1}{Q} \sum_{0 \leq j \leq q} a_d (f, i) \tag{10}$$

Similarly, the output width of the CD-th channel can be expressed as:

$$C_d^q (q) = \frac{1}{Q} \sum_{0 \leq j \leq F} a_c (j, q) \tag{11}$$

The second step is attention generation, which captures the relationship between product image space and model channel by using the location information of defects in industrial products captured by information embedding operation, and accurately obtains the region of interest of product image. It is assumed that the nonlinear activation function is represented by ξ, the horizontal and vertical feature maps in the spatial information of product images are represented by g, and the spatial dimension mosaic operation is represented by []. The two independent tensors obtained by decomposing spatial dimensions are represented by g^f and g^q respectively, and the corresponding convolution transformations are represented by G_f and G_q respectively. The following formula gives the expression of attention generation based on the shared 1×1 convolution transformation function:

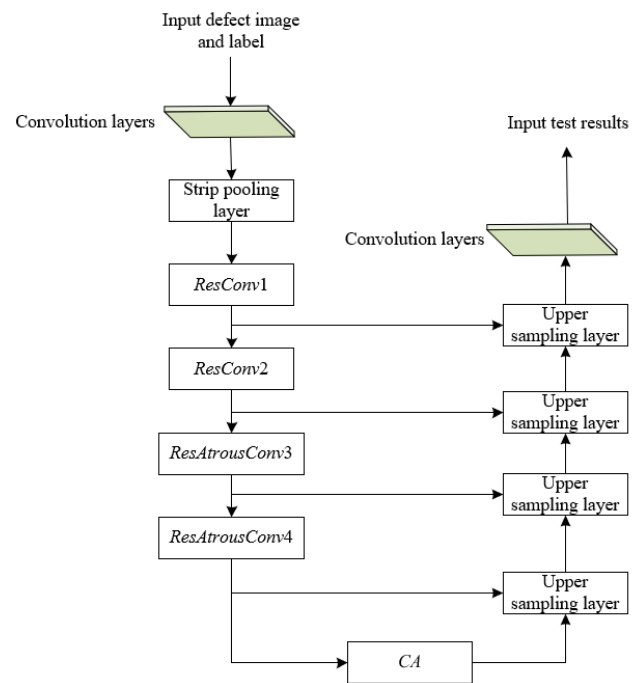$$g = \xi \left(G_1 \left(\left[c^f, c^q \right] \right) \right) \tag{12}$$

Figure 3. Network structure

Assuming that the horizontal and vertical outputs are represented by h^f and h^q, the calculation formula is as followed:

$$h^f = \xi \left(G_f \left(g^f \right) \right) \tag{13}$$

$$h^q = \xi \left(G_q \left(g^q \right) \right) \tag{14}$$

The final output of the CA can be obtained by:

$$b_d(i,j) = a_d(i,j) \times h_d^f(i) \times h_d^q(j) \qquad (15)$$

Figure 3 shows the schematic diagram of the overall network structure.

4. DEFECT MEASUREMENT

The larger the defect length is, the greater the probability of structural problems is. In this article, the centerline method is used to quantify the defect length, and the fitting function of the defect center skeleton is integrated, and the integral result is the cumulative length of all curves. The length of the whole defect can be judged by the following formula:

$$g(a,b) = \begin{cases} 1, if \ (a,b) \in skeleton \ line \\ 0, otherwise \end{cases} \qquad (16)$$

Assuming that the i-th pixel point is represented by a_i, the length K_d of the defect can be calculated by the following formula:

$$K_d = \sum_{i=1}^{m} a_i \qquad (17)$$

The defect area can be quantified by counting the number of pixel points with a gray value of 1. It is assumed that the

geometric calibration index is represented by $g(a,b)$ and the finite pixel area of the defect is represented by dR. The calculation formula is given by the following formula:

$$R_d = \int_R g^2(a,b) dR \cong \sum g^2(a,b) dR \qquad (18)$$

The larger the average width of defects is, the more serious the damage of products is. Assuming that the length of defects is represented by K and the area of defects is represented by R_d, the following formula gives the calculation formula of defect width:

$$\overline{C} = \frac{R_d}{K_d} \qquad (19)$$

5. EXPERIMENTAL RESULTS AND ANALYSIS

According to the five sources of casting, polishing, electroplating, machining or welding and assembly, the apparent types of defects in five industrial products are classified. In this article, the defect detection models are classified and trained based on these five apparent types. Sample set 1, sample set 2, sample set 4 and sample set 5 of defect classification sample sets are trained before and after thinning respectively. Table 1 gives the evaluation results on test samples of classification model of industrial production product defect performance.

Table 1. Evaluation results on test samples of classification model of industrial production product defect performance

Evaluation indicators		TP	FP	FN	P	R	F1
Before thinning	Sample set 1	514	82	112	85.37%	74.51%	85.26%
	Sample set 2	132	6	6	91.42%	93.28%	91.04%
	Sample set 3	3629	142	247	94.35%	97.04%	99.36%
	Sample set 4	1427	369	305	75.62%	71.35%	71.35%
	Sample set 5	958	158	162	81.35%	89.51%	82.19%
After thinning	Sample set 1	2651	147	458	91.24%	84.27%	92.41%
	Sample set 2	2048	75	169	95.68%	96.85%	98.35%
	Sample set 3	3205	162	205	97.43%	91.27%	94.57%
	Sample set 4	3927	13	2	90.51%	98.52%	96.15%
	Sample set 5	3417	184	51	96.85%	91.47%	90.42%
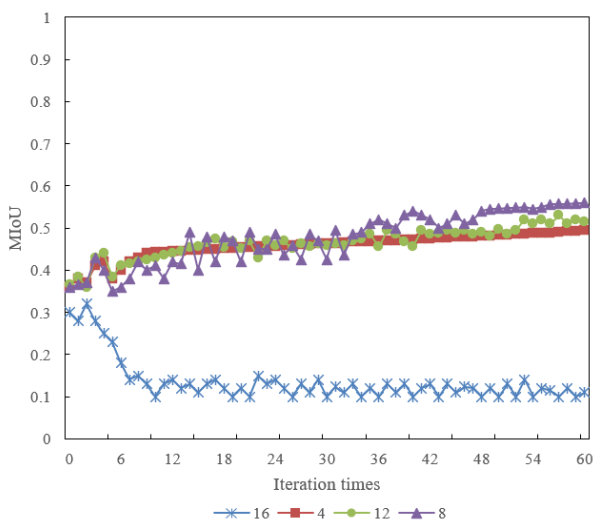
Figure 4. Effect of step threshold on model performance
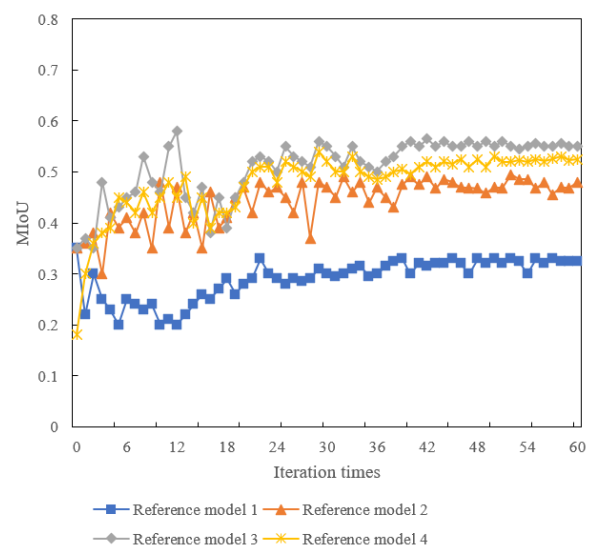
Figure 5. Impact of network architecture on model performance

It can be seen from the table that, except that the recall rate of the test samples trained after thinning of sample set 2 is slightly lower than that before thinning, all the evaluation indexes of the test samples trained after thinning are not lower than that before thinning, mainly because the number of test samples in sample set 2 is small, which leads to the defect detection performance of the model not really appearing. Therefore, it can be seen that preprocessing the industrial production image sample set based on image thinning can effectively improve the generalization ability of the model for product defect detection.

Step threshold is another key parameter that directly affects the image thinning effect. In order to obtain the relatively optimal value of the step threshold, four step thresholds are set respectively, namely 4, 8, 12 and 16. The experimental results of each training model on the test samples are given in Figure 4. It can be seen that when the threshold value is equal to 8, the defect detection performance of the trained model is the best. When the threshold value is 4 and 12, the defect detection ability of the trained model has little difference, while when the threshold value is 16, the MIoU of the trained model rises briefly with the increase of iteration times, and then falls back quickly. Therefore, the threshold of step size selected in this article is 8.

Because this article chooses U-Net network as the infrastructure to build and optimize the product defect detection model, in order to verify the effectiveness of this network architecture, this article sets up a comparative experiment, and takes *ResNet*18, *ResNet*50 and *VGG*16 respectively as reference backbone networks to participate in the defect detection performance comparison with this model. The experimental results of four network architectures are given in Figure 5. It can be seen from the figure that the experimental results of U-Net network selected in this article are relatively better than those of other network architectures.

Table 2. Relevant parameters of each sample corresponding to the model

|	Sample set 1	Sample set 2	Sample set 3	Sample set 4	Sample set 5
Iteration times	62	69	62	67	63
Basic network	U-Net	U-Net	U-Net	U-Net	U-Net
Batch size	64	64	64	64	64
Step threshold	8	8	8	8	8
Image resolution	152×147	152×147	152×147	152×147	152×147
Momentum	0.2	0.4	0.2	0.8	0.6
Total data volume	15824	14274	10368	11257	13629
Proportion of training, verification and test samples	63/25/27	63/25/27	63/25/27	63/25/27	63/25/27
MIoU of test samples	0.52	0.47	0.53	0.21	0.72

Table 3. Comparison of defect detection accuracy before and after model optimization

Model	*Precision*	*Recall*	*F*1	Training time/*s*
Before introducing residual structure	0.3281	0.3571	0.3614	/
Before introducing the hole convolution module	0.7249	0.7365	0.7958	0.34
Before introducing the stripe pooling module	0.6515	0.7051	0.6362	0.31
Before introducing the attention mechanism module	0.7362	0.7648	0.7347	0.33
Final model	0.8519	0.8385	0.8361	0.39

Table 2 gives the relevant parameters of the corresponding model of each sample. It can be seen from the table that the MIoU of defects finally identified by the model trained by sample set 5 with respect to test samples is obviously higher than that of other sample sets, which is related to the simple background and obvious defect characteristics of sample set 5. However, because of the small contrast between the defect area and the surrounding area in sample set 4, the MIoU is lower, the MIoU of defects in the model trained by sample set 1, sample set 2 and sample set 3 is 0.52, 0.47 and 0.52 respectively, all of which are about 0.5, which verifies that the image quality of industrial products collected by machine vision system determines the accuracy of defect detection of the model and also shows the necessity of thinning the image.

Table 3 gives the comparison results of defect detection accuracy before and after model optimization. Through quantitative evaluation indexes, the six models are compared in four indexes: Precision, Recall, F1 and training time. The comparison results are given in Table 3. It can be seen from the table that the accuracy, recall rate and F1 score of automatic detection of product defects in this article are better. In the same calculation time, the final model after introducing the attention mechanism module has higher accuracy than the model before introducing the attention mechanism module.

In order to further test the performance of the built product defect detection model, this article calculates four indexes of defect length, area, average width and maximum width based on 100 sample images according to the proposed method. Figure 6 shows the comparison between the measured results and the real results of pixel-level defect parameters. It can be seen from the four charts that the measured values of the four indexes are distributed from the unfolding points along the center line. The relative error range of calculation is [0.04, 0.22], and the calculation effect basically reaches the expectation.
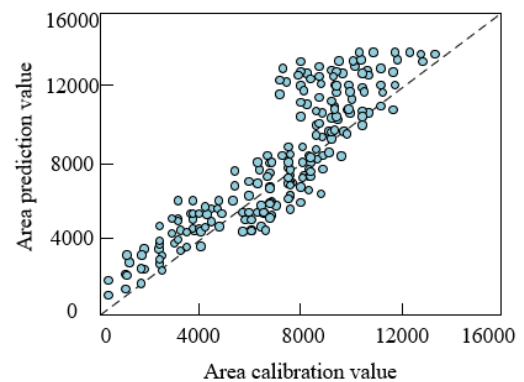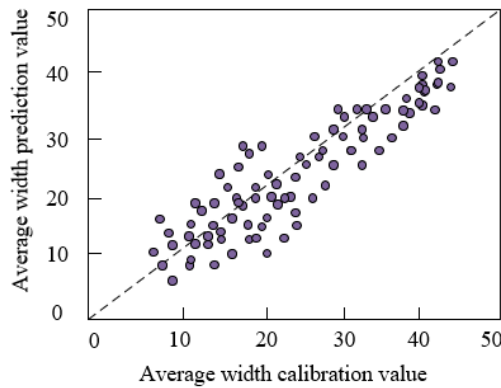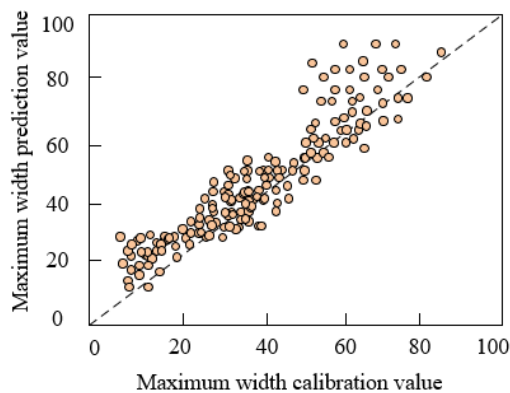

(1)
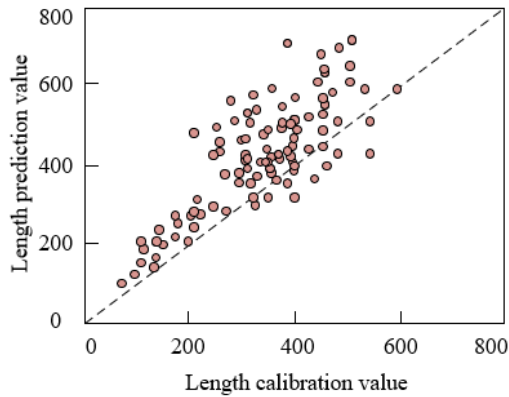
(2)

(3)

(4)

Figure 6. Comparison between prediction results and real results of pixel-level defect parameters

6. CONCLUSION

This article studies the industrial production defect detection method based on machine vision technology in industrial Internet of Things. Firstly, in the second chapter, the images of industrial products collected by machine vision system are preprocessed and thinned to obtain more ideal detection accuracy and measurement accuracy. The methods of image binarization, morphological processing, thinning and burr elimination are given in detail. In the third chapter, product defect detection model is constructed based on U-Net network, and residual structure, hole convolution module, strip pooling module and attention mechanism module are introduced to optimize the network model. Combined with experiments, the evaluation results on test samples of classification model of industrial production product defect

performance are given. It is verified that image thinning can effectively improve the generalization ability of the model for product defect detection. Given the influence of step threshold on model performance, the step threshold is selected as 8. Given the influence of network architecture on model performance, it verifies the effectiveness of selecting U-Net network as infrastructure to build product defect detection model. The relevant parameters of each sample corresponding to the model are given. It is verified that the image quality of industrial products collected by machine vision system determines the accuracy of defect detection of the model. It also shows the necessity of thinning the image. The comparison results of defect detection accuracy before and after the model optimization are given, which further verifies the effectiveness of the constructed model for product defect detection. Finally, based on 100 sample images, the defect length, area, average width and maximum width are calculated according to the proposed method, and the calculation results basically meet the expectations.

REFERENCES

[1] Saleh, M., Jhanjhi, N.Z., Abdullah, A., Saher, R. (2022). Proposing encryption selection model for IoT devices based on IoT device design. In 2022 24th International Conference on Advanced Communication Technology (ICACT), 210-219. https://doi.org/10.23919/ICACT53585.2022.9728914

[2] Hail, M.A.M., Dietrich, L., Fischer, S. (2022). LogStack: A smart logging stack approach for IoT devices based NDN (IoT-NDN). In 2022 International Conference on Software, Telecommunications and Computer Networks (SoftCOM), 1-6. https://doi.org/10.23919/SoftCOM55329.2022.9911233

[3] Habeeb, F., Szydlo, T., Kowalski, L., Noor, A., Thakker, D., Morgan, G., Ranjan, R. (2022). Dynamic data streams for time-critical IoT systems in energy-aware IoT devices using reinforcement learning. Sensors, 22(6): 2375. https://doi.org/10.3390/s22062375

[4] Gherbi, C. (2021). Internet of things and heterogeneous networks technologies: Concepts, challenges and perspectives. Ingénierie des Systèmes d'Information, 26(4): 403-408. https://doi.org/10.18280/isi.260408

[5] Song, S., Zhang, A. (2020). IoT data quality. In Proceedings of the 29th ACM International Conference on Information & Knowledge Management, 3517-3518. https://doi.org/10.1145/3340531.3412173

[6] Sahour, A., Boumehrez, F., Benouaret, M., Mokhneche, A. (2021). Greenhouse climate controller by using of internet of things technology and fuzzy logic. Instrumentation Mesure Métrologie, 20(1): 29-38. https://doi.org/10.18280/i2m.200105

[7] Kumar, N.S., Chandrasekaran, G., Rajamanickam, K.P. (2021). An integrated system for smart industrial monitoring system in the context of hazards based on the Internet of Things. International Journal of Safety and

Security Engineering, 11(1): 123-127. https://doi.org/10.18280/ijsse.110114

[8] Song, L. Z., Zhu, J., Liu, S. T., Qu, Z. J. (2022). Recent Fire Safety Design of High-Rise Buildings. Journal of Urban Development and Management, 1(1): 50-57. https://doi.org/10.56578/judm010106.

[9] Ali, O., Ishak, M.K. (2020). Bringing intelligence to IoT edge: Machine learning based smart city image classification using microsoft azure IoT and custom vision. Journal of Physics: Conference Series, 1529(4): 042076. https://doi.org/10.1088/1742-6596/1529/4/042076

[10] Singh, P., Suryawanshi, M.S., Tak, D. (2019). Smart fleet management system using IoT, computer vision, cloud computing and machine learning technologies. In 2019 IEEE 5th International Conference for Convergence in Technology (I2CT), 1-8. https://doi.org/10.1109/I2CT45611.2019.9033578

[11] Lucas Pascual, A., Madueno Luna, A., de Jódar Lázaro, M., Molina Martinez, J.M., Ruiz Canales, A., Madueno Luna, J.M., Justicia Segovia, M. (2020). Analysis of the functionality of the feed chain in olive pitting, slicing and stuffing machines by IoT, Computer Vision and Neural Network Diagnosis. Sensors, 20(5): 1541. https://doi.org/10.3390/s20051541

[12] Lee, W. (2017). 3D machine vision in IoT for factory and building automation. In 2017 IEEE International Symposium on Circuits and Systems (ISCAS), 1-1. https://doi.org/10.1109/ISCAS.2017.8050234

[13] Sieck, N., Calpin, C., Almalag, M. (2020). Machine vision smart parking using internet of things (IoTs) in a smart university. In 2020 IEEE International Conference on Pervasive Computing and Communications Workshops (PerCom Workshops), 1-6. https://doi.org/10.1109/PerComWorkshops48775.2020.9156121

[14] Duan, H., Xu, X. (2022). Create machine vision inspired by eagle eye. Research, 2022: Article ID 9891728. https://doi.org/10.34133/2022/9891728

[15] Huang, H., Kono, D., Toyoura, M. (2022). Vision-based vibration measurement of machine tool. Journal of Advanced Mechanical Design, Systems, and Manufacturing, 16(1): JAMDSM0014. https://doi.org/10.1299/jamdsm.2022jamdsm0014

[16] Zhang, H., Ma, S., Li, M., Jiang, H., Li, J. (2022). Recent reviews on machine vision-based 3D reconstruction. Recent Patents on Mechanical Engineering, 15(1): 12-24. https://doi.org/10.2174/2212797614666210308123252

[17] Lu, C., Li, Z., Shi, S., Peng, S. (2022). Research on target defect detection based on machine vision. In Journal of Physics: Conference Series, 2219(1): 012060. https://doi.org/10.1088/1742-6596/2219/1/012060

[18] Jin, J., Zhang, X., Fu, X., Zhang, H., Lin, W., Lou, J., Zhao, Y. (2021). Just noticeable difference for deep machine vision. IEEE Transactions on Circuits and Systems for Video Technology, 32(6): 3452-3461. https://doi.org/10.1109/TCSVT.2021.3113572

[19] Yan, Y., Li, H. (2022). Machine vision-based method for estimating lateral slope of structured roads. Sensors, 22(5): 1867. https://doi.org/10.3390/s22051867

[20] Zuo, Z. (2022). Space modeling design art of suspense movies based on machine vision. Mobile Information Systems, 2022: Article ID 8149182. https://doi.org/10.1155/2022/8149182

[21] Zhang, K., Zhu, Y., Wang, W., Zhang, J. (2022). Measurement for blade edge based on machine vision. In New Approaches for Multidimensional Signal Processing, 139-150. https://doi.org/10.1007/978-981-16-8558-3_10

[22] Nakkina, T.G., Vinayaka, M., Masad, A., El Mansori, M., Bukkapatnam, S. (2022). Smart defect identification for manufacturing applications. Surface Topography: Metrology and Properties, 10(3): 035045. https://doi.org/10.1088/2051-672X/ac9247

[23] Teo, H.C., Hashim, U.R., Ahmad, S., Salahuddin, L., Ngo, H.C., Kanchymalay, K. (2022). Efficacy of the image augmentation method using CNN transfer learning in identification of timber defect. International Journal of Advanced Computer Science and Applications, 13(5): 107-114. https://doi.org/10.14569/IJACSA.2022.0130514

[24] Chen, Y., Kang, Y., Feng, B., Li, Y., Cai, X., Wang, S. (2022). Automatic defect identification in magnetic particle testing using a digital model aided de-noising method. Measurement, 198: 111427. https://doi.org/10.1016/j.measurement.2022.111427